

Evolution of the Cluster Mass Function: Gpc^3 Dark Matter Simulations

Paul Bode, Neta A. Bahcall, Eric B. Ford, and Jeremiah P. Ostriker
Princeton University Observatory, Princeton, NJ 08544-1001

ABSTRACT

High-resolution N-body simulations of four popular Cold Dark Matter cosmologies (LCDM , OCDM , QCDM , and tilted SCDM), each containing $\sim 10^5$ clusters of galaxies of mass $M_{1.5} > 5 \times 10^{13} h^{-1} M_\odot$ in a Gpc^3 volume, are used to determine the evolution of the cluster mass function from $z = 3$ to $z = 0$. The large volume and high resolution of these simulations allow an accurate measure of the evolution of cosmologically important (but rare) massive clusters at high redshift. The simulated mass function is presented for cluster masses within several radii typically used observationally ($R = 0.5, 1.0$, and $1.5 h^{-1} \text{Mpc}$, both comoving and physical) in order to enable direct comparison with current and future observations. The simulated evolution is compared with current observations of massive clusters at redshifts $0.3 \lesssim z \lesssim 0.8$. The $\Omega_m = 1$ tilted SCDM model, which exhibits very rapid evolution of the cluster abundance, produces too few clusters at $z \gtrsim 0.3$ and no massive clusters at $z \gtrsim 0.5$, in stark contradiction with observations. The $\Omega_m = 0.3$ models— LCDM , OCDM , and QCDM —all exhibit considerably weaker evolution and are consistent with current data. Among these low density models, OCDM evolves the least. These trends are enhanced at high redshift and can be used to discriminate between flat and open low density models.

The simulated mass functions are compared with the Press-Schechter approximation. Standard Press-Schechter predicts too many low mass clusters at $z = 0$, and too few clusters at higher redshift. We modify the approximation by a simple parameterization of the density contrast threshold for collapse, which has a redshift dependence. This modified Press-Schechter approximation provides a good fit to the simulated mass functions.

Subject headings: galaxies:clusters:general – cosmology:theory – dark matter – large-scale structure of universe

1. Introduction

The local abundance of clusters of galaxies places a powerful constraint on cosmological parameters: $\sigma_8 \Omega_m^{0.5} \simeq 0.5$, where σ_8 is the rms mass fluctuation on an $8h^{-1}\text{Mpc}$ scale and Ω_m is the present cosmological density parameter (Henry & Arnaud (1991), Bahcall & Cen (1992), White, Efstathiou, & Frenk (1993), Eke, Cole, & Frenk (1996), Viana & Liddle (1996), Kitayama & Suto (1997), Pen (1998)). This constraint, while powerful, is degenerate in Ω_m and σ_8 . The evolution of cluster abundance with redshift, especially for massive clusters, breaks this degeneracy (e.g., Peebles, Daly, & Juszkiewicz (1989), Ouk-

bir & Blanchard (1992, 1997), Eke, Cole, & Frenk (1996), Viana & Liddle (1996), Bahcall, Fan, & Cen (1997), Fan, Bahcall, & Cen (1997), Carlberg, Yee, & Ellingson (1997), Henry (1997, 2000), Bahcall & Fan (1998), Eke, et al. (1998), Donahue & Voit (1999)). The evolution of high-mass clusters is strong in $\Omega_m = 1$, low- σ_8 Gaussian models, but is much weaker in low-density, $\sigma_8 \sim 1$ models. Therefore, the evolution of cluster abundance provides one of the most powerful methods to determine both Ω_m and σ_8 . Various analyses using this method have shown that the relatively high abundance of observed clusters to $z \lesssim 0.8$ indicates that the mass-density of the universe is

low: $\Omega_m \sim 0.2 - 0.5$, and $\sigma_8 \sim 1$ (see references above). However, the total number of clusters currently studied at high redshifts is still small, and the model comparisons are generally based on the Press-Schechter (1974) approximation which, while surprisingly accurate, is known to have biases. Direct comparisons with simulations have also been used, but these are generally too small to find the rare high-mass clusters, especially at large redshifts. New observations are currently underway to determine more precisely the evolution of cluster abundance using optical, X-ray, Sunyaev-Zel'dovich, and gravitational lensing surveys. At the same time, larger and more accurate cosmological simulations are needed in order to accurately determine the expected mass function of clusters of galaxies and its evolution with time, in order to allow for proper comparison with the upcoming observations.

In this paper we present gigaparsec-scale simulations of four popular CDM models which allow an accurate determination of the evolution of the cluster mass function from redshift $z = 3$ to $z = 0$, including the rare and cosmologically powerful massive clusters. The rapid increase of available computing power and new algorithms which run efficiently on parallel machines make possible a combination of large simulation volume and high resolution. For comparison, the models presented here are of a larger volume than the Governato et al. (1999) simulations, and attain considerably higher resolution than the Virgo “Hubble Volume” simulations (Evrad 1998; Jenkins et al. 2000). Furthermore, we are able to cover several different models, including the first large volume, high resolution simulation of tilted $\Omega_m = 1$ as well as a quintessence model.

The aim of this paper is to provide the foundation for comparisons with the upcoming observations. Thus the evolution of the mass function is presented in a manner that can be directly compared with observations, using cluster masses within a variety of specific radii typically used in observations, rather than using the not so easily observable virial mass. We discuss the simulations and the method of cluster selection in §2. The evolution of the resulting cluster mass function is presented in §3. Comparison with the Press-Schechter approximation is made in §4, and effects of resolution are discussed in §5. Comparisons with current

observations are shown in §6, and conclusions are summarized in §7.

2. Creating the Simulated Mass Function

2.1. The N-body Simulations

Four currently favored variants of the CDM model were chosen, with parameters consistent with numerous observational constraints (Bahcall et al. 1999). These observations tend to favor a low density universe with $\Omega_m \simeq 0.3$; in addition to spatially flat (LCDM) and open (OCDM) models we include a quintessence model (QCDM). Like LCDM, the QCDM is made spatially flat by including a component with negative pressure, but the Q component is dynamically evolving and spatially inhomogeneous (Caldwell, Dave, & Steinhardt 1998). The equation of state of the Q component, $w = -2/3$, was chosen to be in the range favored by observations (Wang et al. 2000). A standard $\Omega_m = 1$ CDM model was also run, with a strongly tilted power spectrum so as to avoid over-production of present-day clusters. All models are normalized (by σ_8) to match the observed present-day cluster abundance and be consistent with the COBE microwave background normalization. The cosmological parameters for the different runs are listed in Table 1.

The transfer function for a given model was computed using the CMBFAST code (Seljak & Zaldarriaga 1996), modified to handle a dynamical energy component in the QCDM case (Caldwell, Dave, & Steinhardt 1998). The resulting power spectrum was used to generate initial conditions by perturbing particles on a rectilinear grid; this step was performed with the COSMICS software package (Ma & Bertschinger 1995; Bertschinger 1995). Each simulation was begun at a redshift when the RMS density fluctuation was 15%. For QCDM, the fluctuations in the Q component are negligible by the time the simulation begins ($z \approx 30$). Thus, once the matter power spectrum has been computed, the Q component has an effect only through the overall expansion factor $a(t)$.

All four runs contained $512^3 = 134$ million particles in a periodic cube. For the $\Omega_m = 0.3$ runs the box length is $1000h^{-1}\text{Mpc}$; in the SCDM run it is smaller, such that the volume is reduced by a factor of 0.3 relative to the other models (see Table 1). With this choice of parameters all mod-

TABLE 1
MODEL PARAMETERS

Model	Ω_m	Ω_Λ	Ω_b	Ω_{CDM}	h_{100}	n	σ_8	L^a
LCDM	0.30	0.70	0.040	0.260	0.67	1.0	0.90	1000
OCDM	0.30	0.00	0.040	0.260	0.67	1.0	0.80	1000
QCDM	0.30	0.70 ^b	0.040	0.260	0.67	1.0	0.84	1000
SCDM	1.00	0.00	0.076	0.924	0.50	0.625	0.50	669.4

^abox length in $h^{-1}\text{Mpc}$

^bactually a Q component with $w=-2/3$

els, including SCDM, have an individual particle mass of $6.2 \times 10^{11} h^{-1} M_\odot$. Also, the spline kernel softening length in all cases is $\epsilon = 27 h^{-1} \text{kpc}$; thus there is the same mass and force resolution in all the models, simplifying comparisons. The spatial resolution is comfortably smaller than the $\sim 100 h^{-1} \text{kpc}$ characteristic core size of clusters, and the high mass resolution assures that two body relaxation is unimportant in the cluster cores.

The N-body evolution was carried out with the TPM code (Bode, Ostriker, & Xu 2000). The simulations ran on a 128 processor SGI Origin 2000 at NCSA (as part of the Grand Challenge Computational Cosmology Partnership); a single run took 11 to 14 hours to complete. A mesh with 512 cells on a side was used for long-range interactions, while interactions internal to dense peaks were computed with a tree code. The time step for the Particle-Mesh portion of the code is set such that in a given step 1) the cosmological expansion factor a changes by less than 1%, and 2) no particle being evolved solely by the PM code moves more than 1/10 the cell size. Each tree has its own, possibly smaller, time step. This was set such that, for at least 97.5% of the particles in the tree, the time step was shorter than $0.05 * \text{MAX}(\rho_c^{-0.33}, \epsilon) / \text{MAX}(v, v_{rms})$, where ρ_c is the density of the cell containing the particle and v_{rms} is the rms velocity of the entire simulation. The LCDM run took 469 PM steps from $z = 24$ to $z = 0$, and the most massive tree (which contains one of the denser peaks) took 1887 steps.

In the TPM code, only cells above a given den-

sity threshold ρ_{thr} are treated at full resolution, so care must be taken to deal only with objects which lie above this limit. The density threshold parameter was set to $\rho_{\text{thr}} = 0.9\bar{\rho} + 4.0\sigma$, where σ is the dispersion of the cell densities; since σ rises over time, ρ_{thr} is initially only slightly larger than $\bar{\rho}$ and becomes larger as structure forms (see Bode, Ostriker, & Xu (2000)). The evolution of ρ_{thr} is similar in the three $\Omega_m=0.3$ models, rising from $3\bar{\rho}$ at $z=10$ to $10\bar{\rho}$ at $z=1$; at $z=0$, $\rho_{\text{thr}} = 17\bar{\rho}$ for LCDM and slightly less for the other two models. Since structure formation happens later in the SCDM model, ρ_{thr} is much lower, rising from $4\bar{\rho}$ at $z=1$ to $11\bar{\rho}$ at $z=0$. In this paper we consider collapsed objects above $5 \times 10^{13} h^{-1} M_\odot$, or 80 particles within a radius smaller than the code cell size, which implies a density well above ρ_{thr} at all times. In the LCDM run, the smallest object picked out for full resolution treatment contained 28 particles at $z=0.5$ and 42 particles at $z = 0$; the other runs located even smaller objects. Thus we are confident that resolution is not a problem for the objects we are considering. This will be discussed further in §5.

The present models are the largest high-resolution N-body simulations of OCDM, QCDM, and tilted SCDM models currently available. Compared to the Virgo “Hubble Volume” simulations of LCDM and τ CDM (Evrard 1998; Jenkins et al. 2000), the simulated box size L_{box} of these models is a third smaller, but mass and force resolution is superior by a factor of three. Governato et al. (1999) have carried out an OCDM model with cosmological parameters similar to the run

presented here and mass resolution a factor of three higher, but with $L_{\text{box}} = 500h^{-1}\text{Mpc}$. In §5 we will discuss one additional higher resolution run of the LCDM model, which uses more than 10^9 particles.

2.2. Cluster Selection

Once a simulation is complete, it is necessary to identify collapsed objects; this section describes the algorithm used to identify clusters. For a given cluster we are interested in locating the total mass within a set radius $R_c \sim 1h^{-1}\text{Mpc}$, either comoving or physical.

We begin by creating a list of possible cluster centers, using the HOP package developed by Eisenstein & Hut (1998). This code calculates a density for each particle, and associates particles with nearby neighbors possessing a higher density; thus a particle at a density maximum becomes the nucleus of a group. HOP tends to break up larger clusters into a number of smaller groups; we do not attempt to reunite these with the REGROUP portion of the HOP package but instead all group positions are treated as potential cluster centers. However, groups with less than 25 particles or with central density $\rho_c < 180$ are eliminated, because including them in the analysis only results in more poor clusters with mass less than $2 \times 10^{13}h^{-1}M_\odot$, well below our mass threshold.

Nearby pairs of clusters are merged together, working out to a separation of $1h^{-1}\text{Mpc}$; the position of a merged cluster is set to that of the denser of the two progenitors. After this merging is complete, the position of each cluster is revised to the center of mass of all particles located within $1h^{-1}\text{Mpc}$ of the original position. Using this final set of cluster positions, all particles within a specified radius R_c of a cluster center are assigned to that cluster. If a particle is within R_c of multiple clusters, it is assigned to the group to which it has a greater binding energy (using the previously computed mass and central position of each group).

Note that these cluster masses, defined specifically within a fixed radius R_c (for example $R_c = 1.5h^{-1}\text{Mpc}$) are not the same as virial cluster masses. For a rich cluster with $R_{\text{vir}} > 1.5h^{-1}\text{Mpc}$ (where R_{vir} is the radius containing a mean density of 178 times the critical value), $M_{1.5}$ will be smaller than the virial mass and for poor sys-

tems $M_{1.5}$ will be larger than the virial mass when $R_{\text{vir}} < 1.5h^{-1}\text{Mpc}$. Using a fixed R_c facilitates a proper comparison with observations, since the virial radius cannot easily be determined observationally.

3. Evolution of the Cluster Mass Function

Using the selection criteria of §2.2, the cluster mass function (MF), which represents the number density of clusters above a given mass threshold, is determined from the simulations as a function of redshift for $z = 0, 0.17, 0.5, 1, 2$, and 3. At $z = 0$, approximately 10^5 clusters with $M_{1.5} > 5 \times 10^{13}h^{-1}M_\odot$ are located within the simulation volume. The MF is determined for cluster masses within different radii— $R_c = 0.5, 1$, and $1.5h^{-1}\text{Mpc}$, both comoving and physical—in order to explore the dependence of the MF on this scale, as well as provide for proper comparisons with different observations.

The cluster MF is presented in Figure 1 for the four models studied. The cluster mass used here is the mass within the ‘standard’ $1.5h^{-1}\text{Mpc}$ comoving radius, frequently used in observations. At $z = 0$, all models yield the same MF, designed to be consistent with observations; this consistency is essentially forced by the selected σ_8 normalization of each model (Bahcall and Cen 1992, White et al. 1993, Eke et al. 1996, Pen 1998). The models are thus degenerate (by construction) at $z \sim 0$, at least for the richer clusters (SCDM shows many more poor clusters). At higher redshifts, a negative evolution of the cluster MF is seen in all models, as expected, reflecting the growth of clusters with time from small density fluctuations (e.g., Press & Schechter 1974, Peebles 1993, Eke et al. 1996, Fan et al. 1997).

The *rate* of the evolution, however, is strongly model dependent; it breaks the degeneracy seen at $z \simeq 0$. The $\Omega_m=1$ tilted SCDM model, with much stronger evolution, predicts orders-of-magnitude fewer clusters at high redshift than do the low-density models. For example, for a given mass the abundance of clusters in SCDM at $z = 0.5$ is comparable to the abundance at $z = 1$ in the low-density models. Similarly, the number of $z = 1$ clusters in SCDM is comparable to the number of $z = 2$ clusters in the low-density models. At $z = 0.5$, the abundance of Coma-like clusters (with

$M_{1.5\text{com}} \simeq 6 \times 10^{14}h^{-1}M_{\odot}$) is 100 times larger in the low-density models than in SCDM. This large effect, occurring at relatively low redshifts of $z \simeq 0.5 - 1$, provides a powerful method for determining Ω_m and σ_8 from the observed abundance of high-redshift massive clusters. The dependence of the cluster abundance on Λ is much weaker; it becomes more significant at higher redshifts ($z \gtrsim 1$) (e.g. Eke et al. 1996, 1999, Bahcall et al. 1997, Fan et al. 1997).

The LCDM and QCDM mass functions evolve at roughly the same rate, consistent with the prediction of Wang & Steinhardt (1998). OCDM evolves somewhat slower; the differences become more pronounced at $z > 1$. This can be quantified by considering the ratio of cluster abundance $n(z = 1)/n(z = 0)$ for clusters of mass $\geq 8 \times 10^{14}h^{-1}M_{\odot}$ (using the best-fit P-S approximation of §4). OCDM with a ratio of 2.2×10^{-3} is roughly double LCDM (1.2×10^{-3}) and QCDM (1.1×10^{-3}). (SCDM is much lower at 6.9×10^{-8} ; see §6). With improved data sets, this will enable a discrimination between flat and OCDM cosmologies (assuming Ω_m is known). The evolution of the cluster MF presented in Figure 1 can be used for direct comparisons with observations.

The analysis presented above is for cluster masses within the standard Abell radius of $1.5h^{-1}\text{Mpc}$ comoving. Many observations, but not all, determine cluster masses within this radius (based on velocity dispersion, gas temperature, or gravitational lensing). Some observations however determine cluster masses within other radii (typically 0.5 or $1h^{-1}\text{Mpc}$). In order to provide proper comparisons with observations, as well as understand the dependence of the MF on the selected radius within which the cluster mass is measured, we investigate the MF evolution for different radii. In Figure 2 we present the evolution of the cluster MF for cluster masses measured within radii of 0.5, 1, and $1.5h^{-1}\text{Mpc}$, both comoving and physical, for each of the four models.

The dependence of the MF evolution on radius is evident in Figure 2. The progression from large to small radii for either the comoving or physical scales reflects mostly a progression from the large cluster mass within $1.5h^{-1}\text{Mpc}$ to the smaller mass contained within $0.5h^{-1}\text{Mpc}$ for the *same* clusters. Therefore, this progression simply shifts the MF to smaller masses as the radius de-

creases (at all redshifts). If the cluster density profile is $\rho(R) \sim R^{-\gamma}$ on these scales, where $3 - \gamma \approx 1$, then the mass inside R is $M(< R) \sim R^{3-\gamma}$ and a similar shift of mass with radius is expected—as is indeed seen in the simulations.

A more interesting trend is seen between comoving and physical radii. The evolution of the MF is much weaker for cluster masses determined within physical radii than for comoving radii. The strong evolution seen for comoving radii is greatly reduced for physical radii because the same mass is contained within the larger physical radius (at high redshift) instead of the smaller comoving radius (since $R_{\text{phy}} = R_{\text{com}}(1+z)$). Therefore, for a fixed cluster mass (as a function of redshift) the use of physical radius represents relatively lower mass clusters at high redshifts as compared with the comoving radius, by a factor of approximately $(1+z)^{3-\gamma}$. Since lower mass clusters are more numerous, there will be more clusters at high redshifts for cluster masses defined within physical radii than within comoving radii, thus yielding considerably weaker evolution for the former. The effect is stronger in low density models, where only mild evolution is seen in physical coordinates. This is mostly due to the fact that for a low density universe evolution is significant from early times until $z \sim \Omega_m^{-1} \sim 3$, when the universe becomes “open” for local observers and both accretion and merging are reduced. In such models, clusters virialize at $z \sim 2$, after which their evolution slows down; in fixed coordinates their properties, including the mass function, approach constancy.

The difference is large; for example, the abundance of Coma-like clusters ($M_{1.5} \simeq 6 \times 10^{14}h^{-1}M_{\odot}$) at $z = 1$ is nearly 100 times larger for $R = 1.5h^{-1}\text{Mpc}$ physical radius than for $1.5h^{-1}\text{Mpc}$ comoving radius. It is therefore essential that observed and simulated clusters be compared using the same radii. The results presented in Figure 2 can be used for comparisons with observations of cluster masses within these different radii.

4. Comparison with Press-Schechter Approximation

In this section we compare the simulation results with the predictions of the Press & Schechter (1974) approximation frequently used (e.g. Eke,

Cole, & Frenk 1996, Fan, Bahcall, & Cen 1997) in the estimation of the number density and mass distribution of collapsed objects. The P-S approximation states that, after smoothing on the appropriate length scale, regions with density contrast above some threshold δ_c will have collapsed and virialized. The spherical collapse model predicts $\delta_c = 1.686$, with a weak dependence on Ω_m and Λ (Eke, Cole, & Frenk 1996; Wang & Steinhardt 1998). Because P-S theory predicts the mass inside a virial radius, and this radius is often used in numerical work, we first compare the standard P-S predictions with the simulated mass function found using HOP. Employing the HOP regrouping algorithm and tracing clusters to an outer overdensity threshold of 160 gives results similar to the Friends-of-Friends (FOF) algorithm with linking parameter 0.2, which is frequently used to analyze numerical simulations (Eisenstein & Hut 1998; Governato et al. 1999; Jenkins et al. 2000). The resulting HOP mass function is shown in Figure 3, along with the P-S prediction. The shape of the standard P-S mass function does not fit the numerical results; it predicts too many low mass clusters and too few higher mass clusters. This is now a well established drawback of the P-S approximation (Gross et al. 1998; Governato et al. 1999; Jenkins et al. 2000). Furthermore, at higher redshifts there are more collapsed objects than predicted by standard P-S.

To explore the comparison in more detail, and to allow for proper comparison with observations, we will use the mass function defined in terms of the observable quantity of mass within a specific radius. Because P-S theory predicts the mass inside a virial radius, an adjustment needs to be made to predict the mass within $1.5h^{-1}\text{Mpc}$. We follow the prescription of Carlberg et al. (1997) relating the top-hat smoothing length to $M_{1.5}$ rather than the virial mass. A slope of $3 - \gamma = 0.6$ is assumed in the relation $M(< R) \propto R^{3-\gamma}$ near the virial radius. This slope is consistent with the mass profile of observed rich clusters (Carlberg, Yee, & Ellingson 1997; Rines et al. 2000). Also, since N-body simulations give results in variance with P-S, we treat δ_c as a free parameter. For a given comoving $M_{1.5}$, δ_c was adjusted so that the P-S prediction for $n(> M_{1.5})$ matched the N-body result at that mass. This was done for all models and redshifts, beginning at the mass of the

tenth most massive cluster and working down to $6 \times 10^{13}h^{-1}M_\odot$.

The resulting δ_c as a function of $M_{1.5\text{com}}$ is shown in Figure 4. It is apparent that the standard P-S approximation (using δ_c from spherical overdensity in linear theory) does not fit the simulations. The cluster abundance depends on δ_c roughly as $\exp(-\delta_c^2/\sigma^2)$, so a higher δ_c means fewer clusters have formed. The δ_c required by the simulation MF varies with mass. In other words, the shape of the standard P-S mass function is incorrect; for the low Ω_m models it predicts too many low mass clusters (since the standard δ_c is not large enough), even if δ_c is fixed to match the high mass clusters ($\gtrsim 2 \times 10^{14}h^{-1}M_\odot$). The tilted SCDM model shows the opposite trend—we are finding more low mass clusters in the simulations than is predicted. This is due to the assumption that $M(< R) \propto R^{0.6}$ in adjusting the virial mass to $M_{1.5}$. For $\Omega_m = 1$ the extrapolation from $1.5h^{-1}\text{Mpc}$ to R_{vir} reaches to radii $< 1h^{-1}\text{Mpc}$ for low mass clusters. Allowing a steeper slope ($M(< R) \propto R$) for smaller SCDM clusters with a virial radius less than $1h^{-1}\text{Mpc}$ yields results similar to those seen in the other models.

A second trend seen in Figure 4 is that δ_c is lower at higher redshifts, showing that there are more collapsed objects at $z > 0$ than predicted by standard P-S. The redshift dependence of δ_c can be parameterized as $\delta_c = \delta_0 + \delta_1/(1+z)$, with δ_0 and δ_1 chosen separately for each model. A linear fit was made to the best values at $M_{1.5\text{com}} = 2 \times 10^{14}h^{-1}M_\odot$, and then the parameters were adjusted slightly to reduce the difference between the P-S predictions and simulations to below 10% across the entire mass range, if possible. The final choices of δ_0 and δ_1 are shown in Table 2. It can be seen that δ_0 is close to the canonical value of 1.68 and that δ_1 is $\lesssim 10\%$ of this value, meaning the z dependence is weak. Figure 5 shows both the N-body MF and the results of the modified P-S formula using the δ_c from Table 2, along with the fractional difference between the two. The simulation data are fit well by this modified P-S relation, to within 10% for $z \lesssim 2$ (or $z \lesssim 1$ and $M > 10^{14}h^{-1}M_\odot$ for SCDM).

An alternative to the simple power-law density profile used here is the proposed universal profile for dark matter halos of Navarro, Frenk, & White (1997) (see also Lokas & Mamon (2000)); the “toy

TABLE 2
BEST-FIT $\delta_c = \delta_0 + \delta_1/(1+z)$

Model	δ_0	δ_1
LCDM	1.60	0.18
OCDM	1.61	0.07
QCDM	1.61	0.13
SCDM	1.53	0.09

model” of Bullock, et al. (2000) provides the mass and redshift dependence of the concentration. In order to test whether including this dependence would improve the analytic fit, the above analysis was repeated using the NFW profile to adjust the virial mass to $M_{1.5}$. No improvement in the fit was seen; δ_c shows both mass and redshift dependence in a manner similar to that observed using the power-law profile, and the fit is somewhat worse for redshifts $z \gtrsim 2$.

Our results are in agreement with Governato et al. (1999), who likewise found the best fit δ_c to be slightly lower as redshift increases. However, the z dependence found here is weaker. Governato et al. (1999) simulated an open model with parameters close to our OCDM run, and found $\delta_c \approx 1.65$ at $z=1$, agreeing well with our value. However, at $z=0$ the Governato et al. (1999) value is well above ours; this may be due to the fact that their σ_8 value is higher as well.

5. A Higher Resolution Run

An additional simulation was carried out using the same parameters as the LCDM run, except with 1024^3 particles, allowing an examination of the effect of increasing the numerical resolution. The increased number of particles reduces the mass of particle by a factor of eight to $7.75 \times 10^{10} h^{-1} M_\odot$; the softening length was chosen to be $13.6 h^{-1} \text{kpc}$. The run took 800 PM steps and up to 9000 tree steps. This simulation was carried out on a 256 processor SGI Origin 2000 at NCSA and took 9.5 days; the considerable computational expense precludes further runs of this size. For comparison, the $N = 1024^3$ Virgo “Hubble Volume” LCDM simulation (Jenkins et al. 2000; Evrard 1998) contained 27 Gpc 3 , with particle

mass $2.25 \times 10^{12} h^{-1} M_\odot$ and Plummer softening length $100 h^{-1} \text{kpc}$.

A comparison of the mass functions found in the 512^3 and 1024^3 runs is shown in Figure 6. It can be seen that for $z < 2$ the results are similar, the main difference being that the higher resolution run yields slightly more lower mass clusters: at $5 \times 10^{13} h^{-1} M_\odot$, there is a 10% difference. For typical rich clusters, with mass $\gtrsim 10^{14} h^{-1} M_\odot$, the effect is negligible. The modified Press-Schechter prediction, using δ_c as given in Table 2, is also shown. At $z = 0$, the simulation and modified P-S mass functions are within 5% of each other down to $n(> M_{1.5}) = 10^{-7} h^3 \text{Mpc}^{-3}$ (that is, when there are more than 100 clusters in the simulation volume). At higher redshifts the modified P-S prediction yields roughly 10% fewer low mass clusters than the 1024^3 simulation. Since increasing mass resolution by a factor of eight and doubling force resolution has only a minor effect, we feel confident the results presented here will not be changed significantly by increasing resolution.

6. Comparison with Observations

The evolution of cluster abundance is compared with observations in Figure 7. Here we plot the abundance of massive clusters, above a given mass threshold, as a function of redshift. We use the most distant observed massive clusters since such clusters provide the most powerful test of cosmological evolution: these massive clusters cannot exist at high redshifts in $\Omega_m = 1$ Gaussian models; they were simply not formed yet (e.g., Peebles 1993, Fan et al. 1997, Bahcall and Fan 1998, Donahue et al. 1999). The clusters we use are the same as those used by Bahcall & Fan (1998): MS 0016+16, 0451-03, and 1054-03. These clus-

ters are at $z = 0.55$ and $z = 0.83$, with masses above a threshold of $M_{1.5\text{com}} \geq 8 \times 10^{14} h^{-1} M_{\odot}$. They have measured velocity dispersion ($\sigma_r \gtrsim 1200 \text{ km/s}$), gas temperature ($T \gtrsim 8 \text{ Kev}$), strong S-Z decrements (Carlstrom 1998), and (in 2 of the 3 clusters) gravitational lensing mass determinations. Also shown are clusters at $z = 0.38$ from the temperature function of Henry (2000). The temperature has been converted to $M_{1.5\text{com}}$ using the *observed* M-T relation: $M(\leq 1h^{-1}\text{Mpc}) = kT(\text{keV}) \times 10^{14} h^{-1} M_{\odot}$, with the minor extrapolation to $R_{1.5\text{com}}$ following the observed cluster mass profile (Hjorth, Oukbir, & van Kampen (1998), Bahcall & Fan 1998, Bahcall & Sette 2000). The scatter in this observed relation is $\pm 25\%$.

The model predictions are presented by the curves in Figure 7. The shaded horizontal band indicates the range where only a single cluster is expected to be found in the simulation box; below this band, where no clusters can be found, we extrapolate the $n(z)$ curve with our modified P-S approximation (§4) as shown by the lighter curves. The comparison with observations is powerful: no massive clusters are found in the $\Omega_m = 1$ simulations at any redshifts $z > 0.2$! A few clusters are found in the $\Omega_m = 0.3$ simulations at $z \sim 0.6$ and 0.8, consistent with observations. The fact that such massive clusters exist in the universe at $z \simeq 0.8$ and 0.6 rules out $\Omega_m = 1$ Gaussian models at a very high significance level: if $\Omega_m = 1$, 10^{-5} clusters would be expected in the observed survey volume at $z \simeq 0.8$ while 1 cluster is observed; 10^{-3} clusters would be expected at $z \simeq 0.6$ while 2 are observed; and 4×10^{-2} clusters expected at $z \simeq 0.4$ while 2 are observed. Equivalently, based on the observed density, the simulation box should contain 10 such massive clusters at $z \simeq 0.8$ and 10 clusters at $z \simeq 0.6$, while the $\Omega_m = 1$ simulation contains no clusters; from the modified P-S extrapolation one would expect only 10^{-4} and 10^{-2} clusters, respectively. In the $\Omega_m = 0.3$ simulations, on the other hand, we find 1 cluster in the simulation box at $z = 0.8$ and 3 clusters at $z = 0.6$. An even better match with the observed cluster abundance would be achieved with a somewhat lower Ω_m value of ~ 0.2 (e.g., Bahcall & Fan 1998). We note that the observed cluster abundance at $z=0.5-0.8$ could be even higher than used above if the observational surveys are incomplete; this would further reduce the best fit value

of Ω_m .

The models with $\Omega_m \simeq 0.3$ (LCDM, QCDM, OCDM) provide a good fit to the data. While a precise value of Ω_m needs to await a larger and improved sample of massive high redshift clusters, the current data—the existence of just a few massive clusters at high-redshift—already shows that (for Gaussian models) the mass density of the universe is low: $\Omega_m \sim 0.3$. These conclusions from direct large-scale simulations reinforce previous estimates based on the standard P-S approximation (Bahcall et al. 1997, 1998, Carlberg et al. 1997, Henry 1997, 1999, Eke et al. 1998, Donahue et al. 1999, and references therein).

7. Conclusions

Gigaparsec scale high-resolution N-body simulations are used to determine the cluster mass function from $z = 3$ to $z = 0$ for four CDM models: LCDM, OCDM, QCDM, and tilted SCDM. These large, high-resolution simulations, with 10^5 clusters of mass $M_{1.5} \geq 5 \times 10^{13} h^{-1} M_{\odot}$ at the present day, allow an accurate determination of the MF evolution over this redshift range.

The evolution of the mass function is presented for cluster masses within several radii typically used in observations: 0.5, 1, and $1.5h^{-1}\text{Mpc}$, both comoving and physical; this will enable direct comparisons with different observations. The evolution of the MF for clusters of a given mass within a physical radius is found to be considerably weaker than for mass within a comoving radius; this is due to the relatively larger physical radii at high redshift, which means that more numerous poorer clusters are included. After virialization at $z \approx 2$ in the $\Omega_m = 0.3$ models, there is relatively little evolution in physical coordinates. Because of the large differences in the resulting evolution, it is essential that the cluster evolution be compared using the same simulated cluster mass—within the same radius—as observed.

We compare the simulation results with the Press-Schechter approximation; the latter predicts too many low mass clusters at $z = 0$ and too few clusters at higher redshifts. We provide refined parameters for this approximation that best fit the simulations as a function of redshift and mass. With the chosen fits to the overdensity parameter δ_c , the agreement with the simulation MF is

better than 10% for $z \leq 2$ in the three $\Omega_m = 0.3$ models and $z \leq 1$ in SCDM.

We compare the simulation results with current observations of the most massive distant clusters observed to $z \simeq 0.8$. We show that Gaussian $\Omega_m = 1$ models such as tilted SCDM, which predict extremely rapid evolution from $z \sim 1$ to $z \sim 0$, are ruled out at a high significance level; they produce no massive clusters at high redshifts (10^{-5} clusters per the observed volume), in contradiction with observations. Showing much weaker evolution, the $\Omega_m = 0.3$ models—LCDM, OCDM, and QCDM— are all consistent with the data. These results provide one of the most powerful constraints on the mass density of the universe. Upcoming surveys of distant clusters should be able to provide further discrimination between flat (LCDM or QCDM) and open (OCDM) low density cosmologies, since the latter shows relatively weaker evolution.

This research was supported by NSF Grant AST-9803137 (under Subgrant 99-184), and the NCSA Grand Challenge Computational Cosmology Partnership under NSF Cooperative Agreement ASI-9619019, PACI Subaward 766.

REFERENCES

Bahcall, N.A., & Cen, R. 1992, ApJ, 398, L81

Bahcall, N.A. & Fan, X. 1998, ApJ, 504, 1

Bahcall, N.A., Fan, X. & Cen, R. 1997, ApJ, 485, L53

Bahcall, N.A., Ostriker, J.P., Perlmutter, S., & Steinhardt, P.J. 1999, Science, 284, 1481

Bahcall, N.A. & Sette, A. 2000, in preparation

Bertschinger, E. 1995, astro-ph/9506070

Bode, P., Ostriker, J.P., & Xu, G. 2000, ApJS, 128, 561

Bullock, J.S., Kolatt, T.S., Sigad, Y., Somerville, R.S., Kravtsov, A.V., Klypin, A.A., Primack, J.R., & Dekel, A. 2000, MNRAS, in press (astro-ph/9908159)

Caldwell, R.R., Dave, R., & Steinhardt, P.J. 1998, Phys. Rev. Lett., 80, 1582

Carlberg, R.G., Morris, S.L., Yee, H.K.C., & Ellingson, E. 1997, ApJ, 479, L19

Carlberg, R.G., Yee, H.K.C., & Ellingson, E. 1997, ApJ, 478, 462

Carlstrom, J., BAAS, 30

Donahue, M., & Voit, G.M. 1999, ApJ, 523, L137

Eisenstein, D.J. & Hut, P. 1998, ApJ, 498, 137

Eke, V.R., Cole, S., & Frenk C.S. 1996, MNRAS, 282, 263

Eke, V.R., Cole, S., Frenk, C.S., & Henry, P.J. 1998, MNRAS, 298, 1145

Evrard, A.E. 1998, in Evolution of large scale structure: from recombination to Garching, ed. A.J. Banday, R.K. Sheth, L.N. da Costa (Enschede: PrintPartners Ipskamp) 249

Fan, X., Bahcall, N.A., & Cen, R. 1997, ApJ, 490, L123

Governato, F., Babul, A., Quinn, T., Tozzi, P., Baugh, C.M., Katz, N., & Lake, G. 1999, MNRAS, 307, 949

Gross, M.A.K., Somerville, R.S., Primack, J.R., Holtzman, J., & Klypin, A. 1998, MNRAS, 301, 81

Henry, J.P., 1997 ApJ, 489, L1

Henry, J.P., 2000 ApJ, 534, 565

Henry, J.P., & Arnaud, K.A. 1991, ApJ, 372, 410

Hjorth, J., Oukbir, J., & van Kampen, E. 1998, MNRAS, 298, L1

Jenkins, A., Frenk, C.S., White, S.D.M., Colberg, J.M., Cole, S., Evrard, A.E. & Yoshida, N. 2000, preprint (astro-ph/0005260)

Kitayama, T., & Suto, Y. 1997, ApJ, 490, 557

Lokas, E.W., & Mamon, G.A. 2000, preprint (astro-ph/0002395)

Ma, C.-P., & Bertschinger, E. 1995, ApJ, 455, 7

Navarro, J.F., Frenk, C.S. & White, S.D.M. 1997, ApJ, 490, 493

Oukbir, J., & Blanchard, A. 1992, A&A, 262, L21

Oukbir, J., & Blanchard, A. 1997, A&A, 317, 1

Peebles, P.J.E., Daly, R.A., & Juszkiewicz, R. 1989, ApJ, 347, 563

Peebles, P.J.E. 1993, *Principles of Physical Cosmology* (Princeton Univ. Press: Princeton)

Pen, Ue-Li 1998, ApJ, 498, 60

Press, W.H., & Schechter, P. 1974, ApJ, 187, 425

Rines, K., Geller, M.J., Diaferio, A., Mohr, J.J., & Wegner, G.A. 2000, AJ, in press

Seljak, U., & Zaldarriaga, M. 1996, ApJ, 469, 437

Viana, P.P., & Liddle, A.R. 1996, MNRAS, 281, 323

Wang, L., & Steinhardt, P.J. 1998, ApJ, 508, 483

Wang, L., Caldwell, R.R., Ostriker, J.P., & Steinhardt, P.J. 2000, ApJ, 530, 17

White, S.D.M., Efstathiou, G., & Frenk, C.S. 1993, MNRAS, 262, 1023

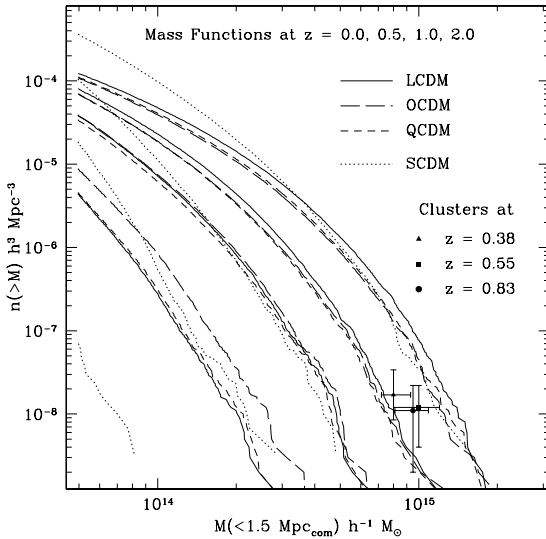
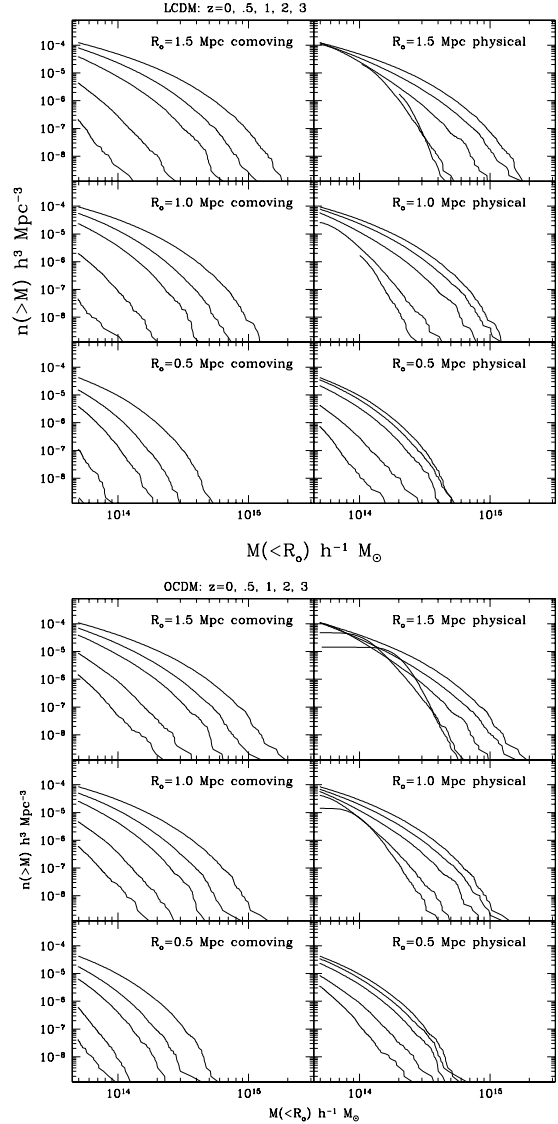


Fig. 1.— The cluster mass functions at redshifts of $z = 0, 0.5, 1.0$, and 2.0 for the four different cosmological models are plotted as lines. Note that

This 2-column preprint was prepared with the AAS L^AT_EX macros v5.0.

the SCDM model (dotted line) at $z = 0.5$ is comparable to the low density models at $z = 1$ and the SCDM model at $z = 1$ is comparable to the low density models at $z = 2$. The three data points with error bars are from observational data discussed in §6.



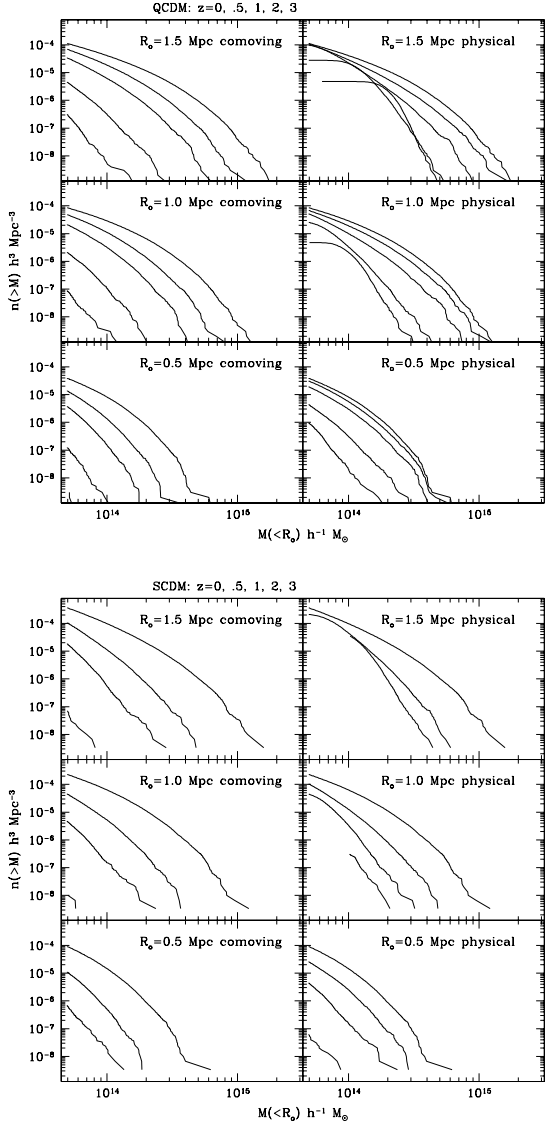


Fig. 2.— The evolution of the cluster MF for cluster masses measured within radii of 0.5, 1, and $1.5 h^{-1} \text{Mpc}$, both comoving and physical, for each of the four models.

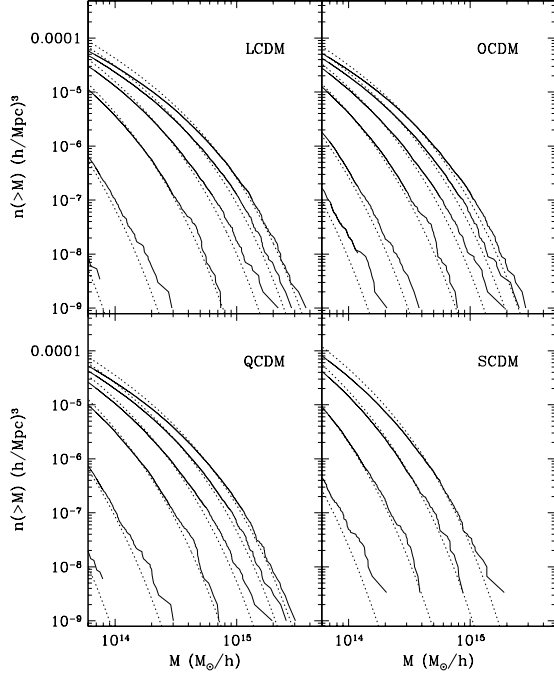


Fig. 3.— Solid lines: the simulated mass function, using masses determined via the HOP algorithm. Dotted lines: Press-Schechter approximation, with δ_c from linear theory. The curves from top to bottom are for redshifts $z = 0, 0.17, 0.5, 1, 2, 3$.

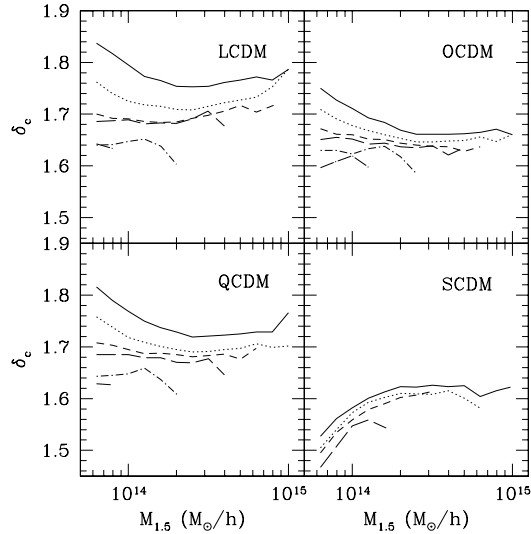


Fig. 4.— The best fit P-S overdensity parameter δ_c as a function of mass. The curves from top to bottom are for redshifts $z = 0, 0.17, 0.5, 1, 2, 3$. Virial mass is translated to mass within comoving $1.5h^{-1}\text{Mpc}$ assuming the observed mass profile $M(< R) \propto R^{0.6}$.

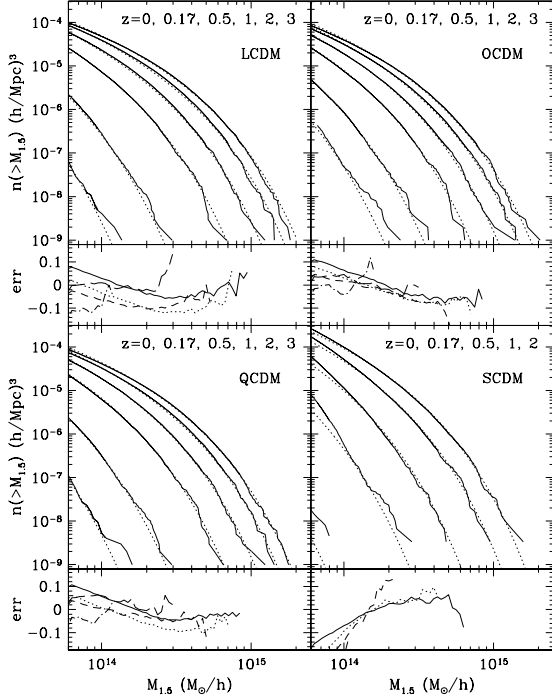


Fig. 5.— The larger panels show the number density as a function of mass from the simulations (solid line) and from the modified P-S approximation (dotted lines) using the overdensity parameter from Table 2. The smaller panel beneath each of these plots shows the fractional difference between the two, $n(\text{PS})/n(\text{sim})-1$. The line types match those in Figure 4.

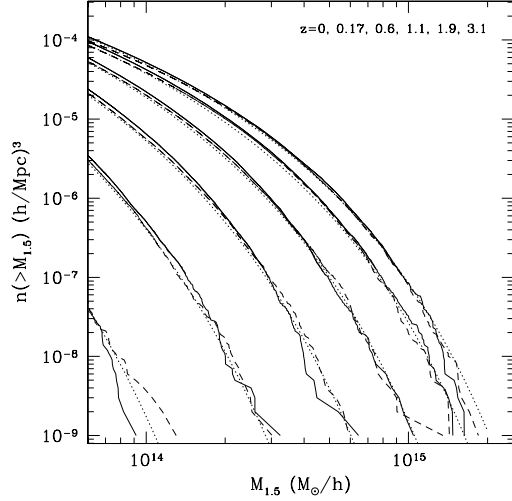


Fig. 6.— A comparison of the mass function in the LCDM model using 512^3 (dashed lines) and 1024^3 (solid lines) particles. Also shown is the modified Press-Schechter prediction (dotted lines), using δ_c as given by Table 2.

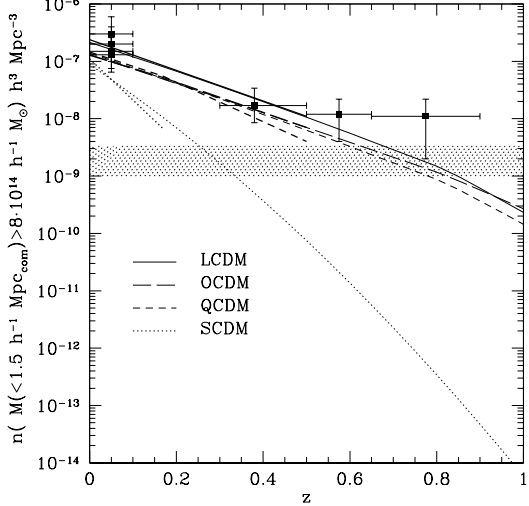


Fig. 7.— The abundance of massive clusters, above a given mass threshold, as a function of redshift. The dark lines are from our numerical simulations, while the light lines are the modified P-S approximations using the parameters from Table 2. The data points are from observations discussed in §6. The dotted region indicates the range of densities for which the numerical simulations would only have one cluster in the entire volume.